JOIV : Int. J. Inform. Visualization, 8(2) - May 2024 724-734

INTERNATIONAL JOURNAL ON INFORMATICS VISUALIZATION

journal homepage : www.joiv.org/index.php/joiv

Evaluation of Joint Technique Iterative Clipping Filtering (ICF) and Neural Network Predistortion on SDR-based MIMO-OFDM System

Melki Mario Gulo [a,*], I Gede Puja Astawa [b], Amang Sudarsono [a], Yoedy Moegiharto [b], Naufal Ammar Priambodo [b], M. Wisnu Gunawan [b]

[a] *Information and Computer Engineering Department, Politeknik Elektronika Negeri Surabaya, Sukolilo, Surabaya, 60111, Indonesia*
[b] *Electrical Engineering Department, Politeknik Elektronika Negeri Surabaya, Sukolilo, Surabaya, 60111, Indonesia*
*Corresponding author: *melkimariogulo@gmail.com*

Abstract*—Multiple-input, multiple-output Orthogonal Frequency Division Multiplexing (MIMO-OFDM) is a communications technology that powers numerous modern communication systems, including 5G and WiFi-6. This technology is utilized in current communication systems due to its high performance and extensive channel capacity. MIMO-OFDM does have disadvantages, such as large Peak-to-Average Power Ratio (PAPR) values. If the signal is processed by a nonlinear Power Amplifier (PA) device, a high PAPR value signal can result in both in-band and out-of-band signal distortion. To combat high PAPR values, PAPR reduction strategies such as Iterative Clipping Filtering (ICF) are utilized. From this study, using ICF with iteration 2 and Clipping Ratios (CR) 3 and 4 can improve the system's minimum Bit Error Rate (BER) by about 22.8% and 91.1%, respectively. Choosing the correct CR will improve the system, but using the lower CR will make it worse than a system without ICF. This occurs in systems using ICF with iterations two and CR 2 and at the same SNR conditions as systems without ICF; using ICF with iterations two and CR 2 results in higher BER values. The use of Predistortion Neural Network (PDNN) can overcome this problem. By using PDNN, there is an improvement in the system where the minimum BER value can reach 0.1×10^{-5}. The percentage decrease in BER from using PDNN for ICF with iterations two and CR 2, 3, and 4 is 99.88%, 99.86%, and 98.807%, respectively. Thus, the joint techniques of ICF and PDNN can significantly enhance the performance of MIMO-OFDM systems with nonlinear PA. Importantly, the experiment was conducted on an SDR device, ensuring the real-world applicability of the results.

***Keywords*— ICF; predistortion; neural networks; MIMO-OFDM; SDR.**

Manuscript received 10 Jul. 2023; revised 10 Dec. 2023; accepted 13 Jan. 2024. Date of publication 31 May 2024.

I. INTRODUCTION

Orthogonal Frequency Division Multiplexing (OFDM) is a telecommunications technology that powers many modern communication technologies, such as 5G and WiFi. OFDM was chosen because of its spectrum efficiency, multipath resistance, and high data rate. This decision is based on the public's desire for improved telecommunications technologies. This technology is utilized to communicate among individuals and has become a significant technology in industry, health, economics, and government. Some real-world applications of 5G and WiFi technologies include IoT [1], [2], e-Health [3], [4]. Intelligent Transportation Systems [5], [6], and others. OFDM technology is sometimes used with multiple-input and multiple-output (MIMO) technology to boost system performance and channel capacity, such as on WiFi-6 and 5G networks. MU-MIMO and OFDMA technologies on WiFi-6 allow several users to use MIMO on the same channel, increasing channel capacity and allowing it to be used in dense areas [7], [8].

Despite having many advantages in adoption in today's communication systems, Multiple-Input Multiple-Output Orthogonal Frequency Division Multiplexing (MIMO-OFDM) also has one downside, which is the high Peak-to-Average Power Ratio (PAPR) value [9], [10], [11], [12]. High PAPR values arise due to the accumulation of peak power on each subcarrier, which can lead to issues when passing through a nonlinear Power Amplifier (PA). Intermodulation distortion can occur, leading to in-band distortions. These distortions can decrease the signal-to-noise ratio (SNR), negatively impacting the MIMO-OFDM system's performance. To address this challenge, PAPR reduction techniques can be applied. The study has already conducted several assessments on PAPR reduction approaches in

MIMO-OFDM [13], [14]. The findings by [13] employed Clipping Least Mean Square (CP-LMS) to conduct PAPR reduction on the MIMO-OFDM system. The LMS algorithm is used to optimize the settings of the clipping process to achieve an optimal reduction in PAPR.

Meanwhile, a study by [14], Iterative Clipping Filtering (ICF) utilized to reduce PAPR on MIMO-OFDM had a superior performance in reducing PAPR compared to Selective Mapping (SLM) approaches. The reduction strategy based on clipping is extensively used in the MIMO-OFDM system since it has low complexity. However, in both experiments, there is a trade-off between the decreased PAPR value and the Bit Error Rate (BER) value. The rise in the BER value resulted from the implementation of clipping techniques (CP-LMS and ICF), which remove peak signals that may cause out-of-band distortion and spectral regrowth. To address this issue, using PAPR reduction techniques can be combined with predistortion (PD).

PD is a technique that can also be utilized to compensate for high PAPR problems on MIMO-OFDM systems. PD has the inverse properties of the PA that can pay for the nonlinear PA. Research on joint PD and PAPR reduction has been carried out previously, as in the studies [15], [16], [17]. The study by [15] applied a combination of PAPR reduction, Partial Transmit Sequence (PTS), and Hammerstein PD techniques to the OFDM system. The study found that adding PD to PTS reduced BER values to as low as 10^{-7} at SNR 11 dB. This was in contrast to PTS, which didn't add PD and only gave BER 10^{-3} at SNR 30 dB. The study by [16] applied ICF PAPR reduction techniques and Hammerstein PD to the OFDM relay system. From this investigation, using PD increased system performance by 15.82% on BER 10^{-5}. Another study by [17] implemented ICF and PD on OFDM-based Software-Defined Radio systems (SDR). In this investigation, ICF succeeded in lowering PAPR by 6.06 dB. In the research [15], [16], the use of joint reduction approaches PAPR and PD and the channel disturbance in the model are still simulated. According to [17], system implementation was still carried out on the transmitter only; hence, no system performance data was available. In the three studies, the OFDM system is still used without MIMO.

A lack of study has been conducted on the joint implementation of PD and PAPR reduction techniques in MIMO-OFDM systems to compensate for higher PAPR values. Indeed, study investigations [15], [16], [17] show that the quality of the OFDM system can be enhanced by employing both a joint PD technique and the PAPR reduction technique instead of relying solely on the PAPR reduction technique. Meanwhile, MIMO-OFDM is widely used in modern transmission systems like WiFi, 4G, and 5G. As a result, this study was conducted to improve the MIMO-OFDM communication system, which had been degraded due to high PAPR values. The joint PAPR reduction technique of the ICF method and Predistortion Neural Network (PDNN) in SDR-based MIMO-OFDM will be evaluated in this study. The selection of ICF for PAPR reduction was based on its minimal computational costs, as demonstrated in studies [15], [16], and this system is executed on SDR devices with limited memory. Neural Network (NN) were selected due to their elastic properties and ability to emulate the inverse characteristics of a model of a sophisticated PA [18]. Furthermore, some studies [19], [20] have established that PDNN performs better than alternative digital PD methods.

This study contributes to applying joint ICF and PDNN methods to SDR-based MIMO-OFDM. This study aims to improve SDR-based MIMO-OFDM, which is degraded by nonlinear PA and has a high PAPR value, by combining ICF and PDNN methods. The gap between this study and the previous study is that this study used a mixed method to improve the SDR-based MIMO-OFDM, while the previous study only used PDNN or PAPR reduction. The joint method of PD and PAPR reduction technique has already been used in several studies in the OFDM system and has gotten a better result than only the PAPR reduction technique. This study combined the PDNN and ICF methods to get better results than the ICF method alone. These techniques reduce spectral regrowth and in-band distortion due to nonlinear PA and ICF while enhancing BER. Furthermore, the feasibility of the system implementation suggested for the SDR device is assessed in a real-world setting. The system evaluation will employ a complementary cumulative distribution function (CCDF) plot, signal constellation, maximal SNR, and BER charts.

II. Materials and Method

Several techniques employed in the proposed system will be covered in this section.

A. MIMO-OFDM

MIMO is a multi-antenna communication system that operates under the same conditions as the equation (1):

$$N_t, N_r > 1 \tag{1}$$

where N_t is the number of transmitters and N_r number of the receivers. There are two methods in the MIMO communication system. These schemes include spatial diversity and spatial multiplexing. The spatial diversity MIMO method improves communication link quality, while spatial multiplexing increases data rate and channel capacity. In several studies, researchers utilized Walsh-Hadamard precoding (WHT) along with MIMO and a spatial multiplexing technique [21], [22], [23]. The goal of precoding in the MIMO spatial multiplexing system is to enable the joint transmission of independent data from each transmitter. The Hadamard matrix of order 2^n is used to produce the WHT matrix, where $n \in \mathbb{N}$. On equation (2), a WHT matrix of order two can be written.

$$H(2) = \begin{bmatrix} 1 & 1 \\ 1 & -1 \end{bmatrix} \tag{2}$$

Order 2^n can be expressed as a recursive equation for the WHT matrix's subsequent generation (3).

$$H(2^n) = \begin{bmatrix} H(2^{n-1}) & H(2^{n-1}) \\ H(2^{n-1}) & -H(2^{n-1}) \end{bmatrix} \tag{3}$$

The precoding procedure is carried out on the MIMO-OFDM spatial system after the modulation but before the demultiplexer procedure. So, if $x(k) = [x_1, x_2, x_3, \dots, x_n]$ Then, precoding the modulated symbol can be expressed as an equation (4).

$$x_p(k) = H(m)_{i,j} \times x(k) \tag{4}$$

where $H(m)$ is the WHT with order m, i is the WHT row, j is the WHT column, and $x_p(k)$ is the symbol of the precoding result. The demultiplexer operation is then performed on $x_p(k)$ with the number of N_t. Demultiplexing is a process of separating a stream symbol into many stream symbols based on the number of transmitters. Fig. 1 depicts the demultiplexing process on MIMO with $N_t = 2$.

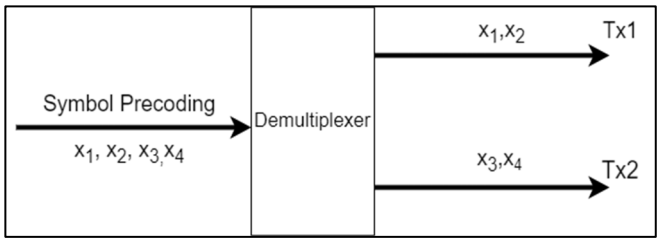

Fig. 1 MIMO Demultiplexer Process $N_t = 2$

Following the demultiplexer process (illustrated in Figure 1), the Inverse Fast Fourier Transform (IFFT) procedure is applied to each transmitter's symbol. The goal of the procedure is to convert the symbol from the frequency domain to the time domain. The IFFT process for MIMO-OFDM can be written in equation (5):

$$x(n) = \frac{1}{N}\sum_{k=0}^{N-1} x_p(k) \,.\, e^{j\left(\frac{2\pi}{N}\right)nk} \quad (5)$$

where N is the number of OFDM subcarriers and $x(n)$ is modulated OFDM signal or the output signal of the IFFT process. The following signal, $x(n)$, will be sent to the receiver and produce an equation for the received signal written in equation (6):

$$\mathrm{y(n)} = \mathrm{hx(n)} + \omega \quad (6)$$

where $y(n)$ is the received signal, h is the channel transmission, and ω is noise on the receiver. The received signal will be subjected to the Fast Fourier Transform (FFT) technique. The signal is put back into the frequency domain using the FFT technique. Equation (7) can be used to represent the FFT procedure:

$$y(k) = \sum_{k=0}^{N-1} y(n) \,.\, e^{-j\left(\frac{2\pi}{N}\right)nk} \quad (7)$$

where $y(k)$ denotes the FFT symbol, and N is the number of the subcarriers. The maximum likelihood algorithm, such as equation (8), is used to multiplex and decode symbols.

$$\hat{x} = \arg\min_{x} \left\| y(k) - \hat{h}.x \right\|^2 \quad (8)$$

where $\hat{h}$ is estimated channel, $y(k)$ is the symbol after FFT process, $\hat{x}$ is a decoded symbol, and x is the transmitted signals obtained from the channel equalization process on equation (9)

$$x = \left(\hat{h}^H \hat{h}\right)^{-1} \hat{h}^H y(k) \quad (9)$$

where $\hat{h}^H$ is Hermitian channel estimation.

B. Peak Average to Power Ratio (PAPR)

One of the drawbacks of MIMO-OFDM is the presence of PAPR, which leads to the transmission of distorted signals while passing through a nonlinear PA. On the MIMO-OFDM subcarrier, PAPR happens when symbols with the same phase overlap. The PAPR value on the MIMO-OFDM system increases with the number of subcarriers. According to research [24], equation (10) can be used to determine the maximum PAPR value for a MIMO-OFDM system:

$$PAPR_{max} = 10 \log_{10} N \quad (10)$$

where N is the number of MIMO-OFDM subcarriers, the maximum PAPR value produced by the system on the MIMO-OFDM system with N=128 is 21.072 dB. Meanwhile, equation (11) can be used to calculate the PAPR value on each subcarrier:

$$PAPR_{dB} = 10 \log_{10} \frac{P_{peak}}{P_{average}} = 10 \log_{10} \frac{\max\left[|x(n)|^2\right]}{E\left[|x(n)|^2\right]} \quad (11)$$

where $x(n)$ is the MIMO-OFDM modulated signal, and $E[.]$ is the expectation operator. Following that, a graph of the CCDF can be utilized to evaluate PAPR values on a MIMO-OFDM system. The CCDF graph will depict the likelihood of a PAPR value compared to a given value. The CCDF equation is written in equation (12):

$$CCDF = P(PAPR > PAPR_0) \quad (12)$$

where $P(.)$ denotes probability and $PAPR_0$ denotes the threshold value of PAPR.

C. Iterative Clipping Filtering (ICF)

ICF is a PAPR reduction technique that works by clipping a peak power value on an OFDM symbol into a power value that matches the threshold that has been configured. ICF is the development of the Clipping Filtering algorithm with the addition of iteration processes during clipping. ICF is used to minimize the peak power symbol MIMO-OFDM so that it does not enter the PA's saturation area. Fig. 2 depicts an illustration of ICF work.

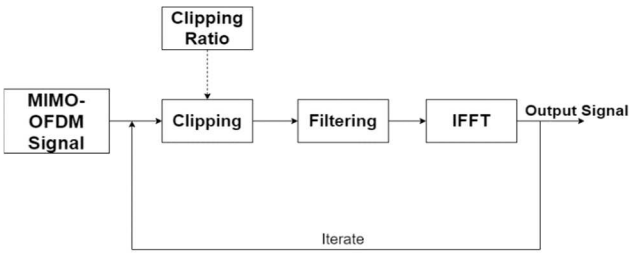

Fig. 2 ICF Block Diagram

The process on the ICF of Figure 2 begins with the clipping process. Clipping is conducted against MIMO-OFDM signals depending on the previously determined CR. The clipping process equation is written on the formula (13) [25]:

$$\hat{x}(n) = \begin{cases} T \times e^{(j \times \theta_n)}, & |x(n)| > T \\ x(n) & , \ otherwise \end{cases} \quad (13)$$

where $x(n)$ is MIMO-OFDM modulated signal, θ_n the phase of $x(n)$, and T is a threshold that the equation can be defined in equation (14):

$$T = CR \times \sqrt{P_{average}} \quad (14)$$

where CR is the clipping ratio, equation (14) clearly shows that using a low CR value results in a lower threshold clipping. Threshold selection becomes crucial in the ICF since a trade-off with the BER is produced, as shown in the research [25].

A signal with a high peak power will also be in the nonlinear PA device saturation region when the threshold value is higher.

D. Power Amplifier (PA)

Graphing the power input data against the power output of the PAs using the AM/AM characteristic curve reveals the nonlinearity of PA. The obtained AM/AM characteristic curve can be modeled using the PA. PA modeling is essential for understanding the PA's relationship between power input and output. Saleh [26], [27], [28] and Rapp [29], [30] are two examples of PA modeling methodologies. The modeling of the Saleh PA type was chosen for this investigation since it is simple in complexity and memoryless. Furthermore, since the system is embedded in SDR devices with limited memory, opting for a method with low complexity or computational cost would be more advantageous. Fig. 3 is an illustration of the PA process.

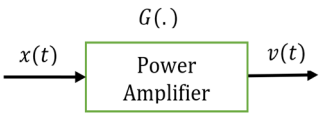

Fig. 3 Illustration of PA

From Figure 3, $x(t)$ is the input signal of PA, $G(.)$ is a modeling function of PA, and $v(t)$ is the output signal of PA. These three parameters can be written into equations (15).

$$v(t) = G\big(x(t)\big) \tag{15}$$

Next, the G function representing PA modeling can be replaced with the modelling approach indicated in the equation (16).

$$G\big(x(t)\big) = \frac{\alpha.x(t)}{1+\beta.x^2(t)} \tag{16}$$

From equation (16), α is the gain of PA, and β is the gain compression from linear area to nonlinear area. The values of the parameters in this study were acquired from the PA modeling performed in paper [31], [32], where $\alpha = 2.1587$ and $\beta = 1.1517$.

E. Predistortion (PD)

PD can be utilized to adjust for nonlinear PAs while eliminating distortions induced by ICF processes with excessively low thresholds. Fig. 4 depicts how PD works.

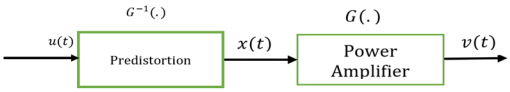

Fig. 4 Illustration of PD

As seen in Figure 4, PD performs signal processing before the PA processes the signal. PD processes signals using the inverse function of PA. The PD process equation before the PA from Figure 4 can be represented in equation (17).

$$v(t) = G\big(x(t)\big) = G(G^{-1}(u(t))) \tag{17}$$

where $u(t)$ is the input signal of PD, $x(t)$ is the output signal of PD, and $G^{-1}(.)$ is a function of PD characteristics. In this study, an NN was used to design a PD. Neural Networks (NN) are employed due to their ability to replicate the inverse characteristics of PA modeling. An NN is developed for PD by utilizing signals from a PA. To develop models of NN that have inverse features of PA, the input model uses the output signal of PA, and the output model utilizes the input signal of PA. The NN equation that makes the PD is written in equations (18–20).

$$y_1 = f(\omega_1 \begin{bmatrix} Real\big(u(t)\big) \\ imag\big(u(t)\big) \end{bmatrix} + b_1) \tag{18}$$

$$y_i = f(\omega_i BN(y_{i-1}) + b_i) \tag{19}$$

$$y_M = f(\omega_M BN(y_{M-1}) + b_M) \tag{20}$$

where ω is weight, b is bias, $f(.)$ is activation function, and BN is batch normalization. Batch normalization is utilized in the NN model to normalize input and enhance the model's ability to generalize. From equations (18–20), the architectural model for NN is created, which can be seen in Fig. 5.

```
_________________________________________________________________
Layer (type)                 Output Shape              Param #
=================================================================
dense (Dense)                (None, 80)                240
_________________________________________________________________
batch_normalization (BatchNo (None, 80)                320
_________________________________________________________________
activation (Activation)      (None, 80)                0
_________________________________________________________________
dense_1 (Dense)              (None, 40)                3240
_________________________________________________________________
batch_normalization_1 (Batch (None, 40)                160
_________________________________________________________________
activation_1 (Activation)    (None, 40)                0
_________________________________________________________________
dense_2 (Dense)              (None, 20)                820
_________________________________________________________________
batch_normalization_2 (Batch (None, 20)                80
_________________________________________________________________
activation_2 (Activation)    (None, 20)                0
_________________________________________________________________
dense_3 (Dense)              (None, 40)                840
_________________________________________________________________
batch_normalization_3 (Batch (None, 40)                160
_________________________________________________________________
activation_3 (Activation)    (None, 40)                0
_________________________________________________________________
dense_4 (Dense)              (None, 80)                3280
_________________________________________________________________
activation_4 (Activation)    (None, 80)                0
_________________________________________________________________
dense_5 (Dense)              (None, 2)                 162
=================================================================
Total params: 9,302
Trainable params: 8,942
Non-trainable params: 360
_________________________________________________________________
```

Fig 5 Neural Networks Model Architecture for PD

The model of NN predistortion shown in Figure 5 comprises a layer input, five hidden layers, and a single output layer. Each hidden layer applies batch normalization. The activation function in this model architecture is the Rectified Linear Unit (ReLU), which can be expressed in equation (21).

$$f(x) = \max(0, x) \tag{21}$$

Then, the training parameters shown in Table I below are applied to train the NN model.

TABLE I
NEURAL NETWORKS TRAINING PARAMETERS

No	Parameter	Value
1	Optimizer	Adam
2	Loss Function	MSE
3	Epochs	30
4	Batch Size	50
5	Total Train Data	800000
6	Total Test Data	200000

F. System Model

Fig. 6 and 7 show the proposed system's transmitter and receiver schematic blocks.

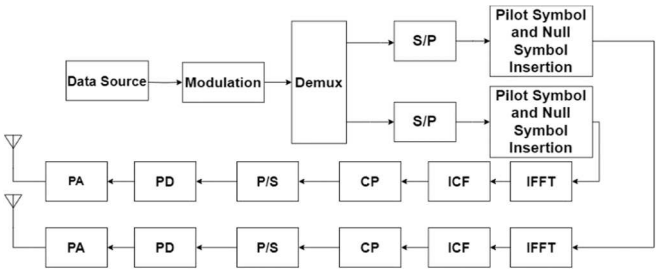

Fig. 6 Transmitter System Block Diagram

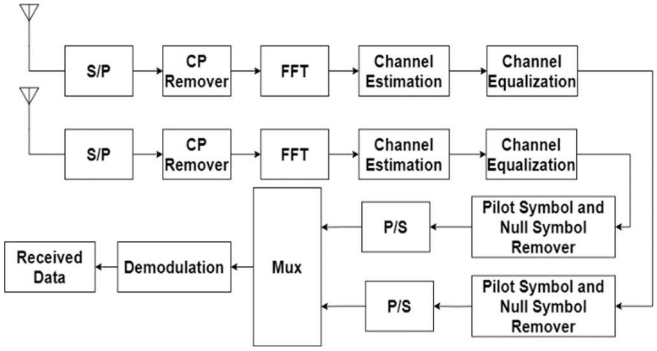

Fig. 7 Receiver System Block Diagram

In Fig. 6, the first process of transmitter systems shows how the data source is initially modified with Quadrature Amplitude Modulation (QAM) to generate the modulated symbol. The successive modulated symbols will be WHT precoded and demultiplexed to divide the stream symbol into multiple streams. The proposed system divides the stream into two parts. The symbol is split into two separate streams, and then a serial-to-parallel technique is employed to break each stream into numerous OFDM symbols, each containing 96 data subcarriers. Then, for 128 subcarriers, add a null symbol of 23 and a pilot symbol of 9. Next, the IFFT is performed to convert the signal to a time domain. The PAPR reduction technique, following the IFFT procedure, employs the ICF to decrease the PAPR value of the MIMO-OFDM signal. A Cyclic Prefix (CP) of 32 is added to the MIMO-OFDM signal to prevent intersymbol interference. Afterward, the signal is converted to a serial format and subjected to PD. PD is employed to mitigate the effects of nonlinear PA and minimize in-band intermodulation distortion caused by ICF. The PA amplifies the final signal before transmitting it to the receiver.

$N_r = 2$ is used on the receiver system shown in Fig. 7. The received signal is transformed into a parallel shape, and the CP is deleted. Next, the FFT technique converts the signal to the frequency domain. The generated IFFT signal will then be processed with channel estimation and channel equalization to equalize the channel. The least squares channel estimate algorithm is used in the estimation step, whereas zero forcing is used in the equalization process. After channel equalization, the pilot and null symbols are eliminated, and the data is transformed into serial form. A multiplexer merges symbols that are already serial into a stream and demodulates them to produce received data during the multiplexing process.

The transmitter system in Fig. 6 and Fig. 7 will then be implemented on a Software Defined Radio (SDR) device of the Universal Software Radio Peripheral (USRP) type. The USRP is a national instrument's SDR device. The MIMO-OFDM system implementation on the USRP device is designed using a block diagram such as Fig. 8.

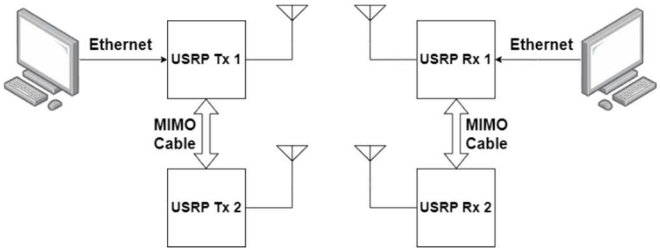

Fig. 8 USRP Block Diagram

From Fig. 8, it can be seen that the transmitter and receiver of the MIMO-OFDM system will use two USRP devices on each side. Two USRP devices on each section are synchronized using a MIMO cable. The intended synchronization is clock and frequency synchronization. In each section, an Ethernet cable connects the USRP and PC. The specifications of the devices utilized in this study can be seen in Table II.

TABLE II
DEVICE SPECIFICATION

No.	Device Name	Specification
1	NI-USRP 2920	Frequency Range : 50MHz – 2.2 GHz Connector: Ethernet
2	Antenna VERT 900	Frequency Range: 824 MHz – 960 Mhz, 1710 MHz – 1990 MHz
3	Transmitter PC	Operating System: Windows 10 RAM: 8GB, Processor: Intel Core i5 8th Gen 2.5 GHz
4	Receiver PC	Operating System: Windows 11 RAM: 16GB, Processor: Intel Core i7 12700H 4.7 GHz

In this research, we used the PC to embed programs on the USRP. LabVIEW and Python programming languages are used to program this system. Python is used to operate and train neural networks for PD, whereas LabVIEW is utilized to program communication operations. Figs. 9 and 10 show the Labview software block used in this study.

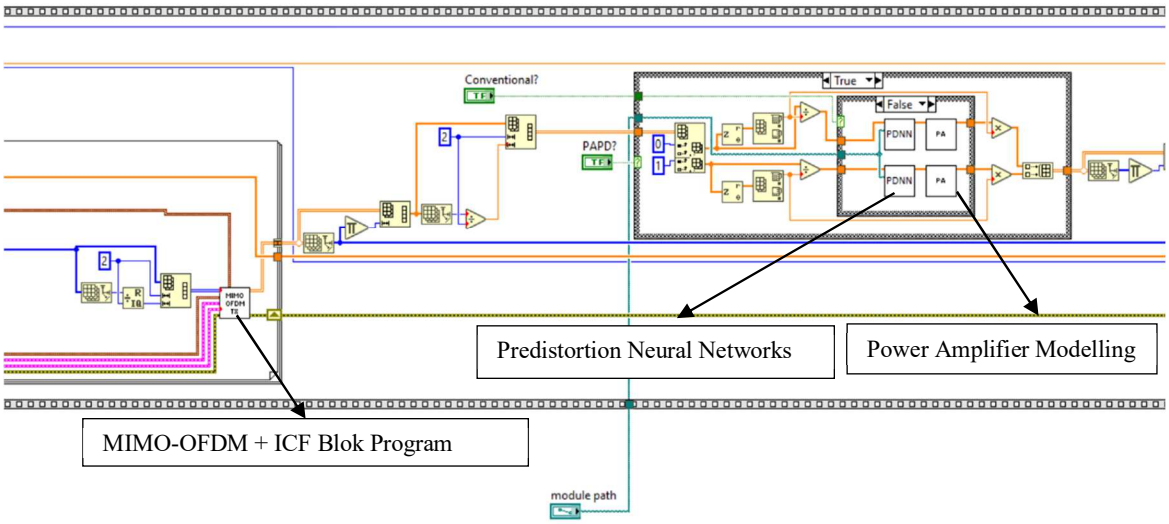

Fig. 9 Transmitter Block Diagram

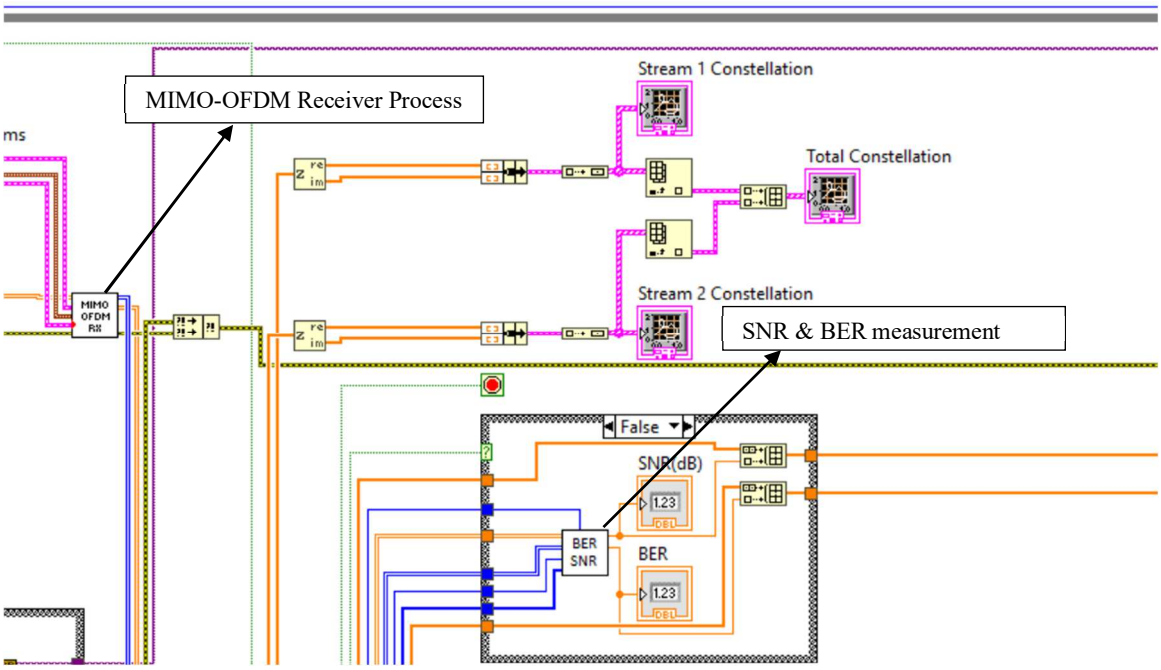

Fig. 10 Receiver Block Diagram

III. Results and Discussion

This section will discuss the assessment of the proposed system. The system was evaluated on the 4th floor of the postgraduate building of Politeknik Elektronika Negeri Surabaya (PENS). This evaluation is conducted with the measurement setup illustrated in Fig. 11. Fig. 11 depicts the measurement of the transmitter and receiver in a line-of-sight (LOS) configuration, with a range of 2 meters. Table III shows the parameters of the MIMO-OFDM transmitter and receiver utilized in evaluating the system. Due to the utilization of real-world channels and noise conditions in this assessment, the resulting evaluation is also real-world rather than a simulation.

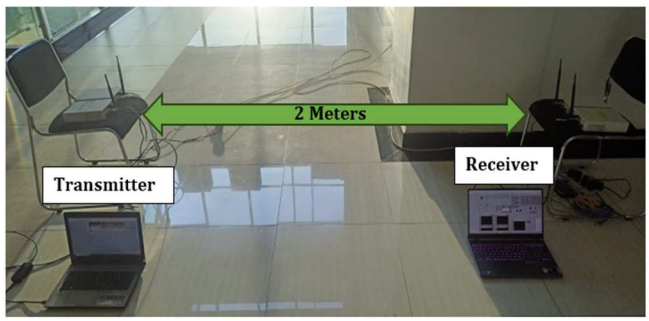

Fig. 11 The setup for system evaluation

TABLE III
EVALUATION PARAMETER SYSTEM

No	Session	Parameter	Value
1	Transmitter	Frequency	915MHz
		N-IFFT	128
		Data symbol	96
		Pilot symbol	9
		Null symbol	23
		CP	32
		IQ Rate	1M
		Antenna	2
		OFDM Symbol	50
		PAPR Reduction	ICF
		PA	Saleh
		PD	Neural Networks
		Modulation	4-QAM
2	Receiver	Channel Equalization	Zero-Forcing
		Channel Estimation	Least Square
		Frame Synchronization	Zadoff-chu
		Antenna	2

A. ICF Evaluation

This section will assess the performance of PAPR ICF reduction on the MIMO-OFDM system with nonlinear PA. The evaluation is carried out by measuring the CCDF charts using equation (12) and constellation signals from the system. The CCDF graph illustrates the correlation between the probability of Peak-to-Average Power Ratio (PAPR) values and a specific threshold value. The measurement scenarios are shown in Table IV.

TABLE IV
EVALUATION SCENARIO OF ICF

No.	Scenario
1	MIMO-OFDM + PA
2	MIMO-OFDM + PA + ICF (Iterartion=2, CR=2)
3	MIMO-OFDM + PA + ICF (Iterartion=2, CR=3)
4	MIMO-OFDM + PA + ICF (Iterartion=2, CR=4)

For the first scenario, we measured the MIMO-OFDM system using PA. In the second scenario, we used PA and the ICF reduction technique with iteration 2 and CR 2. We used PA and the ICF reduction technique in the third scenario with two iterations and a CR of 3. Lastly, we used PA and the ICF reduction technique in the last scenario with two iterations and a CR of 4. For the first examination, we use the CCDF chart shown in Fig. 12. In Fig. 12, scenario 1 produces the most considerable PAPR value. This follows the estimated value of the PAPR in OFDM in equation (10). The most considerable PAPR value in scenario 1 is 19.8762 dB; this value is close to the PAPR estimated value using equation (10) of 21.072 dB on a MIMO-OFDM system with 128 subcarriers.

The CCDF graph shows that the reduction in the maximum PAPR value differs among scenarios, dependent upon the CR value utilized. The maximum PAPR value in scenario 4 decreased by 11.41 dB, approximately 57.4% of the maximum PAPR value in scenario 1.

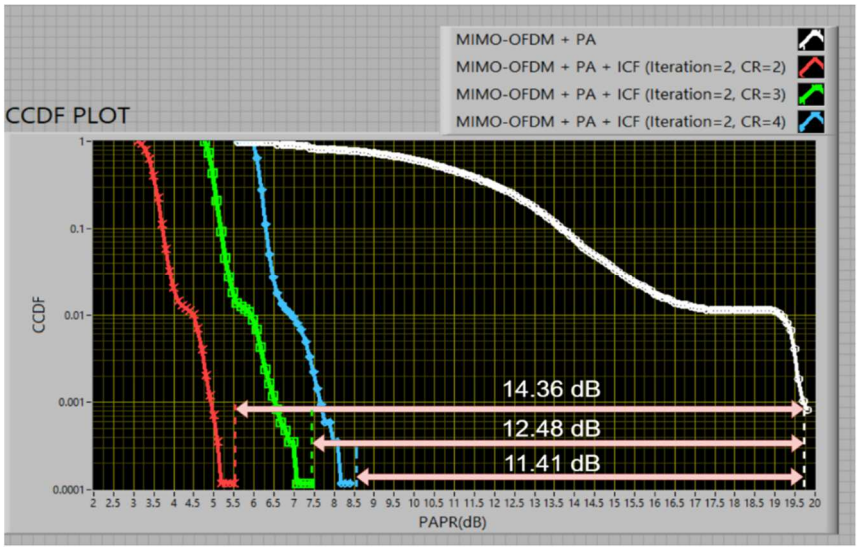

Fig. 12 CCDF Chart

In scenario 3, the maximum value of PAPR decreased by 12.48 dB, equivalent to 62.78% of the maximum value of PAPR in scenario 1. In scenario 2, the maximum value of PAPR decreased by 14.36dB, equal to 72.24% of the maximum value in scenario 1. Scenario 2 has the most significant decrease in PAPR values compared to other scenarios, aligning with the theory stated in the equation (14). The utilization of ICF will result in a reduction of the PAPR value, hence enhancing the signal quality in the MIMO-OFDM system. This is because a high PAPR might result in signal distortion inside the system due to the operation of the Power Amplifier in the nonlinear region.

The following evaluation utilized the constellation plot, SNR, and BER. The SNR Estimation Equation measures the SNR at the receiver, as seen in the equation (22) [33]:

$$\hat{y} = \frac{[\sum_{i=1}^{g}(r_{i_I} m_{i_I} + r_{i_Q} m_{i_Q})]^2}{\frac{\varepsilon_{av}^2}{g}\sum_{i=1}^{g}|r_i|^2 - \varepsilon_{av}[\sum_{i=1}^{g}(r_{i_I} m_{i_I} + r_{i_Q} m_{i_Q})]^2} \quad (22)$$

where $\hat{y}$ is the SNR value in the receiver, $r_{i_I} m_{i_I} + r_{i_Q} m_{i_Q}$ is the received symbol, g is the total symbol, and ε_{av} is the reference symbol. In addition to SNR, the BER value is used to evaluate this system. The BER value equation can be written in equation (23):

$$BER = \frac{Nerr}{Nbits} \quad (23)$$

where $Nerr$ is the total error bit, and $Nbits$ is the total bits from the MIMO-OFDM system receiver for the three scenarios listed in Table IV. Fig. 13, Fig. 14, Fig. 15, and Fig. 16 depict the system receiver's signal constellation.

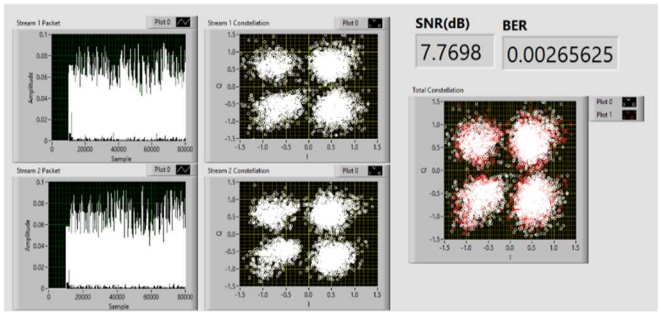

Fig. 13 Received Signal Constellation for Scenario 1 Table IV

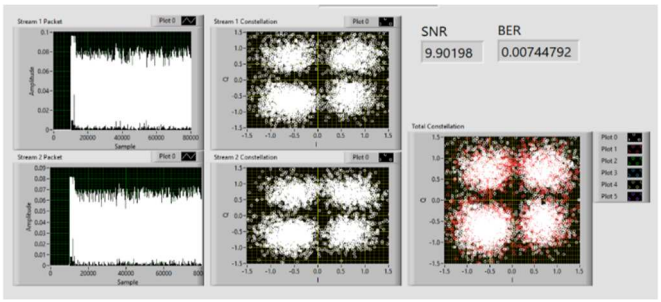

Fig. 14 Received Signal Constellation for Scenario 2 Table IV

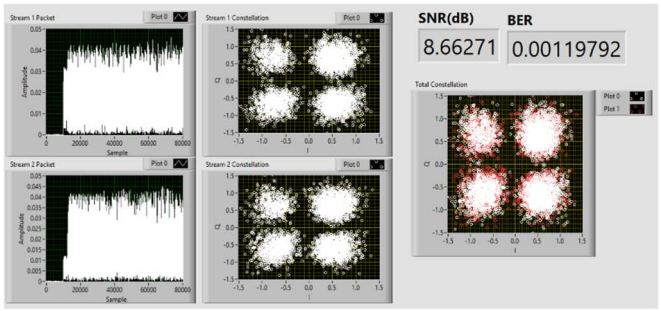

Fig. 15 Received Signal Constellation for Scenario 3 Table IV

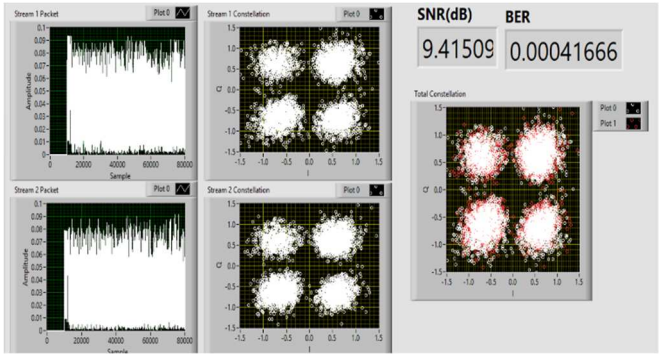

Fig. 16 Received Signal Constellation for Scenario 4 Table IV

From Fig. 13 to Fig. 16, scenario 4 in Fig. 16 produces the best results. This is because the BER value in this scenario can reach 0.4167×10^{-3} when the SNR is 9.415 dB. This BER value is the smallest compared to the BER measurement values in other scenarios. In addition, scenario four can achieve a smaller BER value in lower SNR conditions than the results of scenarios 2 and 3. In this measurement, it can also be seen that scenario 2 produces the worst results, where in this scenario, the BER value is only 0.744792×10^{-2} at SNR 9.90 dB. The value of this scenario is the worst because, with the highest SNR conditions compared to other measurement results, the BER value obtained is the highest compared to different scenarios. In addition, scenario 2, which uses ICF, produces worse measurement values than the system that does not use ICF, namely scenario 1. This can happen because using a minimal CR value will distort the signal. Using ICF with a lower CR yields higher BER values than using ICF with a higher CR. This conforms to the theoretical explanation for the trade-off between system performance BER and PAPR values on the ICF. In addition, although ICF can enhance the system's performance, BER values obtained by the system using ICF cannot achieve a minimum of BER = 0 based on measurement results. This is due to the ICF's distortion and in-band distortions from nonlinear PA, which prevents the BER value from reaching the minimum value. We can also see the distortion caused by nonlinear PA and lower CR ICF on the constellation plot. The constellation plot shows that the signal tends to spread even if they are already grouped into four groups since this study uses QAM modulation. In the following evaluation, the PDNN was integrated with the ICF scenario to improve the SNR, lower the BER values on the receiver, and reduce distortion caused by PA.

B. Evaluation of the joint technique ICF and Predistortion Neural Networks

This session will assess the use of ICF and PDNN together. We will first evaluate the PDNN training results shown on the loss chart and the validation loss against iterations in Fig. 17. Fig. 17 demonstrates that the 30th iteration of the PDNN model's training produced a training loss value of 6.165×10^{-4} and validation loss value of 7.27×10^{-6}. Fig. 18 demonstrates that the training loss and validation loss model values are small enough to generate a robust PDNN model with reverse PA characteristics.

Fig. 18 depicts the AM/AM characteristic of PA, PDNN, and PA-compensated PDNN (PA+PDNN). Fig. 18 demonstrates that PA shows nonlinear characteristics. This nonlinear power amplifier condition leads to distortion within the desired frequency range, resulting in unsatisfactory measurements of SNR and BER, as shown in scenario table IV. The measurements still do not yield optimal results despite implementing the ICF PAPR reduction approach to lower the peak-to-average power ratio (PAPR). Hence, to enhance the SNR and BER results obtained from system measurements, it is necessary to employ PDNN to compensate for the nonlinear effects of the PA. The graph displays PDNN, represented by the orange line, demonstrating the inverse properties of PA. This is achieved by utilizing PA characteristics as input and OFDM signal characteristics as output during the training process, as shown in equation (17). The efficacy of PDNN for PA compensation is demonstrated by the output characteristics of PA+PDNN compensation, depicted in green. The compensation results show a linear relationship between the normalized input and output power. Consequently, the linear working area of the

power amplifier (PA) is extended, resulting in a decrease in in-band distortion. Additional experiments will be conducted utilizing scenario Table V to demonstrate the efficacy of the combined approach of ICF and PDNN in mitigating PA.

Fig. 17 Training Loss and Validation Loss Graph

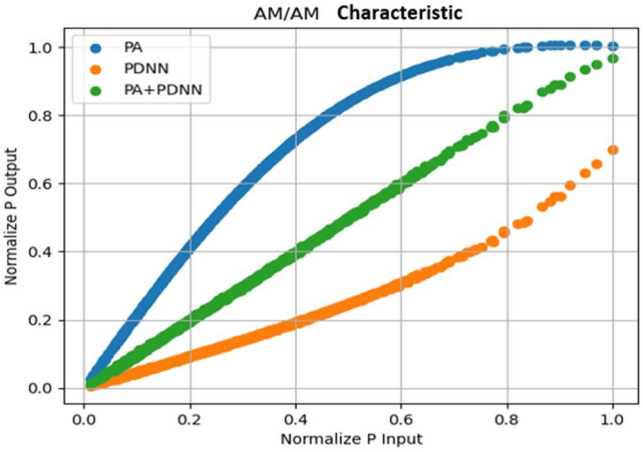

Fig. 18 AM/AM Characteristic Graph

TABLE V
ICF+PDNN EVALUATION SCENARIO

No.	Scenario
1	MIMO-OFDM + PA + PDNN + ICF (Iteration=2, CR=2)
2	MIMO-OFDM + PA + PDNN + ICF (Iteration=2, CR=3)
3	MIMO-OFDM + PA + PDNN + ICF (Iteration=2, CR=4)

Using the constellation chart on the receiver system, the following will be evaluated based on the scenario presented in Table V. Fig. 19, Fig. 20, and Fig. 21 depicts a graph of the receiver constellation system in both scenarios.

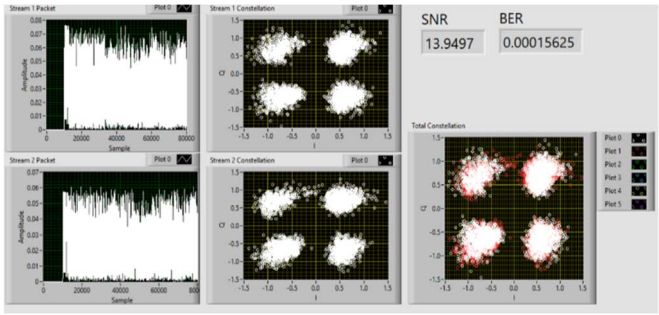

Fig. 19 Received Signal Constellation for Scenario 1 Table V

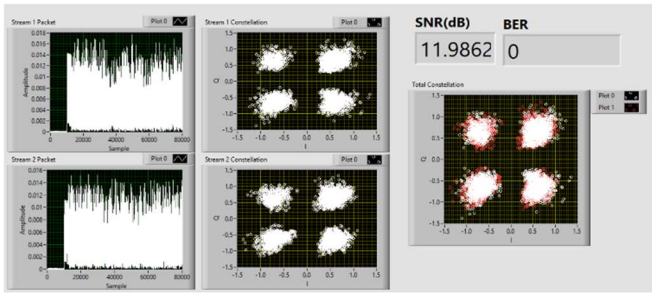

Fig. 20 Received Signal Constellation for Scenario 2 Table V

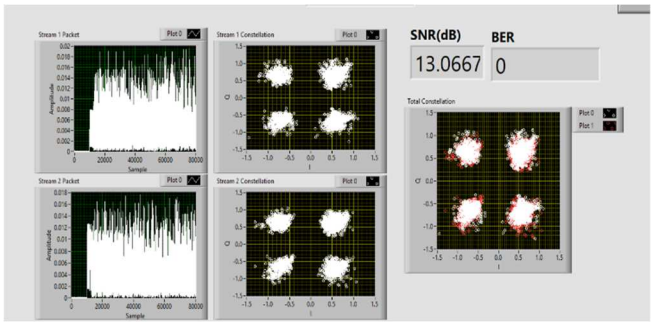

Fig. 21 Received Signal Constellation for Scenario 3 Table V

Figures 19–21 show the results of testing the receiving system. They show that using PDNN in the PAPR ICF reduction method improves the system. In the evaluation of scenario 1, the BER value was 0.15625 10^{-3} at an SNR of 13.94 dB. These results are better than those from Fig. 14. PDNN can increase SNR and reduce BER in this system, which is why these results are considered good. Furthermore, in scenarios 2 and 3, the BER value is 0 for all signal transmissions with signal SNR values of 12.59 dB and 13.60 dB, respectively. These results are also better than using the ICF PAPR reduction technique alone to compensate for the nonlinear PA. From the constellation signal that is received in the receiver system with the join technique PDNN and ICF (Figs. 19–21), it can be seen that the constellation signal is narrower than the constellation signal in the system that only uses ICF or the system without PDNN (Figs. 14–16). Furthermore, we conducted multiple measurements to obtain more stable results in the tested scenario.

To improve the results, we repeat the system evaluation multiple times using the scenarios in Tables IV and V. The repeated evaluation yields the BER vs. SNR chart as an evaluation result. Fig. 23 depicts the system evaluation's BER chart as determined graphically. From the BER chart in Fig. 23, the MIMO-OFDM system with nonlinear PA without ICF and PDNN has a minimum BER value of 0.952×10^{-3} at an SNR value of 9.823 dB. Furthermore, this value increased when ICF was used to reduce the PAPR value in MIMO-OFDM before being processed by PA. When using ICF with iteration 2 with CR 3, the BER value becomes smaller, namely $0.735\times10^{-3,}$ when the SNR is 9.065 dB. Meanwhile, ICF with iterations two and CR 4 produces a BER value of up to 0.838×10^{-4} at an SNR of 10.075 dB. From these results, the percentage reduction in the value of BER due to the use of ICF with iteration 2 CR 3 and CR 4 is 22.8% and 91.1%, respectively.

Meanwhile, in the scenario using ICF with iteration 2 and CR 2, the BER graph is worse than the system without ICF.

The minimum BER value in this scenario is 0.836 $\times 10^{-3}$ at an SNR of 12.22 dB. This value is worse than the system with ICF because getting a BER value of 0.836 $\times$ 10^{-3} requires an SNR value of 12.22 dB. Furthermore, when the SNR value is 9,823 dB, the system without ICF obtains a BER value of 0.952$\times 10^{-3}$, smaller than the ICF iterations two and CR 2, which get a BER value of 0.504 $\times$ 10^{-2}. This is consistent with the trade-off theory between using a smaller CR value and a worse system performance value in research [7] and [8]. The smaller CR in the ICF can cause additional distortion in the MIMO-OFDM system. That's why choosing the correct CR can lead to improvement, but selecting the smaller CR can lead to system degradation. From Figure 23, using PDNN with ICF can improve the system's quality compared to using ICF alone to compensate for high PAPR values and nonlinear PA. This can be seen from the minimum BER value of the joint technique of PDNN and ICF reaching 0.1 $\times$ 10-5 for all scenarios. The percentage decrease in the minimum BER value in each system scenario with ICF compared to systems with PDNN and ICF starting from the ICF iteration 2 CR 2, ICF iteration 2 CR 3, and ICF iteration 2 CR 4 scenarios is 99.88%, 99.86%, and 98.807%. Meanwhile, from all the joint technique PDNN and ICF scenarios, the best scenario is the PDNN scenario with ICF iteration 2 and CR 4 because it can achieve a BER value of 0.1 $\times$ 10^{-5} at a smaller SNR value than the others, which is 9.823 dB.

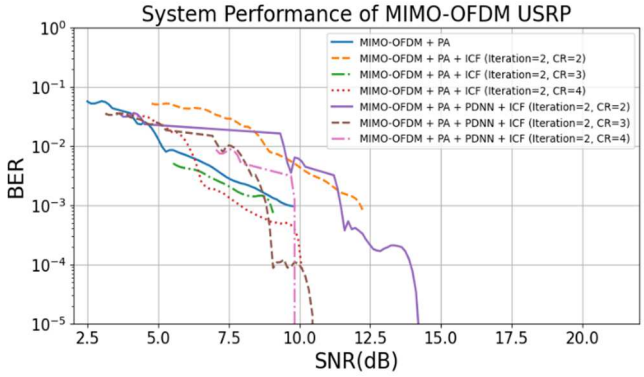

Fig. 22 BER Chart

IV. Conclusions

The study assessed the combination of ICF and PDNN algorithms on MIMO-OFDM systems with a nonlinear PA using USRP. The initial experiment evaluated the efficacy of the ICF PAPR reduction technique in mitigating high PAPR values in MIMO-OFDM signals. Evaluation is conducted by utilizing CCDF charts. The CCDF graph demonstrates that the use of the ICF PAPR reduction technique effectively decreases the high PAPR values in the original MIMO-OFDM signal by 57.4%, 62.78%, and 72.24% with CR values of 4, 3, and 2, respectively, with two iterations. The decrease in the PAPR value impacts the measurement results of the constellation, SNR, and BER values on the receiver of the multiple-input multiple-output orthogonal frequency division multiplexing (MIMO-OFDM) system. Based on the measurements obtained from the MIMO-OFDM receiver system, the implementation of ICF yields the highest SNR value of 9.90 dB when the parameter CR is set to 2. In addition, using ICF also produces the lowest BER value of 0.4167 $\times$ 10^{-3} when the parameter CR is set to 4.

The use of ICF in MIMO-OFDM systems can be further enhanced with the use of PDNN. PDNN will compensate for the nonlinear PA, which decreases in-band distortion in MIMO-OFDM signals. In MIMO-OFDM systems, in-band distortion can be observed in the receiver constellation. This distortion is evident when the system does not employ PDNN. The characteristic feature of this distortion is a scattered or diffuse signal constellation. PDNN has demonstrated its efficacy in achieving nonlinear PA compensation, resulting in a more linear PA signal output from the AM/AM characteristic graph experiments. In addition, the utilization of PDNN combined with ICF enhanced the system, as evidenced by an improvement in the SNR value and a reduction in the BER value in the MIMO-OFDM receiver. By employing this combination strategy, it is possible to enhance the received SNR to a value of 13.94 dB using the parameter CR = 2. In addition to the SNR value, employing this combination technique can decrease the BER value at the receiver to a BER value of 0, utilizing the parameters CR = 3 and 4.

The measuring procedure is iteratively conducted until a graph depicting BER versus SNR is obtained to achieve a more accurate and consistent system performance assessment. This graph illustrates the BER at different SNR conditions until it reaches the minimum BER value. The optimal results of this test are achieved using a MIMO-OFDM system that utilizes a combination of PDNN and ICF algorithms, with parameters CR set to 4 and iteration set to 2. The graph depicting the BER vs. SNR shows that the BER reaches its minimum value of 0.1 $\times$ 10^{-5} at an SNR of 9,823 dB. In contrast, the worst scenario involves a MIMO-OFDM system with ICF parameters CR = 2 and iteration = 2. The worst outcome occurs when the BER values are 0.836 $\times 10^{-3,}$ and the SNR is 12.22 dB. This aligns with prior research indicating that choosing an excessively small CR may result in more distortion in the MIMO-OFDM system. In addition, this study determined that the combination of PDNN and the PAPR ICF reduction technique enhanced the system's quality compared to using solely the PAPR ICF reduction technique.

In future studies, we will conduct a comparative analysis between PDNN and other traditional PD systems to establish the superior performance of PDNN over its counterparts. In addition, we will substitute PA modeling with hardware PA modeling.

Acknowledgment

The authors are also grateful to the Directorate General of Vocational Education Ministry of Education, Culture, Research and Technology for providing financial support for our research. Their funding allowed us to conduct our research and complete our work.

References

[1] S. R. Pokhrel, H. L. Vu, and A. L. Cricenti, “Adaptive Admission Control for IoT Applications in Home WiFi Networks,” IEEE Transactions on Mobile Computing, vol. 19, no. 12, pp. 2731–2742, Dec. 2020, doi: 10.1109/tmc.2019.2935719.

[2] S. Li, L. D. Xu, and S. Zhao, “5G Internet of Things: A survey,” Journal of Industrial Information Integration, vol. 10, pp. 1–9, Jun. 2018, doi: 10.1016/j.jii.2018.01.005.

[3] P. T and S. S. Nayak, “5G Technology for E-Health,” 2020 Fourth International Conference on I-SMAC (IoT in Social, Mobile, Analytics and Cloud) (I-SMAC), Oct. 2020, doi: 10.1109/i-smac49090.2020.9243403.

[4] E. Selem, M. Fatehy, and S. M. A. El-Kader, “E-Health applications over 5G networks: challenges and state of the art,” 2019 6th International Conference on Advanced Control Circuits and Systems (ACCS) & 2019 5th International Conference on New Paradigms in Electronics & information Technology (PEIT), Nov. 2019, doi:10.1109/accs-peit48329.2019.9062841.

[5] L. Guevara and F. Auat Cheein, “The Role of 5G Technologies: Challenges in Smart Cities and Intelligent Transportation Systems,” Sustainability, vol. 12, no. 16, p. 6469, Aug. 2020, doi:10.3390/su12166469.

[6] A. Gohar and G. Nencioni, “The Role of 5G Technologies in a Smart City: The Case for Intelligent Transportation System,” Sustainability, vol. 13, no. 9, p. 5188, May 2021, doi: 10.3390/su13095188.

[7] T. Ahmed B., M. S. Krishnan, and A. K. Anil, “A Predictive Analysis on the Influence of WiFi 6 in Fog Computing with OFDMA and MU-MIMO,” 2020 Fourth International Conference on Computing Methodologies and Communication (ICCMC), Mar. 2020, doi:10.1109/iccmc48092.2020.iccmc-000133.

[8] F. Jiang, Q. Li, and X. Chen, “Channel Smoothing for 802.11ax Beamformed MIMO-OFDM,” IEEE Communications Letters, vol. 25, no. 10, pp. 3413–3417, Oct. 2021, doi: 10.1109/lcomm.2021.3099167.

[9] Y. A. Jawhar et al., “New low-complexity segmentation scheme for the partial transmit sequence technique for reducing the high PAPR value in OFDM systems,” ETRI Journal, vol. 40, no. 6, pp. 699–713, Sep. 2018, doi: 10.4218/etrij.2018-0070.

[10] H. Bao, J. Fang, Q. Wan, Z. Chen, and T. Jiang, “An ADMM Approach for PAPR Reduction for Large-Scale MIMO-OFDM Systems,” IEEE Transactions on Vehicular Technology, vol. 67, no. 8, pp. 7407–7418, Aug. 2018, doi: 10.1109/tvt.2018.2837112.

[11] A. Singal and D. Kedia, “Performance Analysis of MIMO-OFDM System Using SLM with Additive Mapping and U2 Phase Sequence for PAPR Reduction,” Wireless Personal Communications, vol. 111, no. 3, pp. 1377–1390, Nov. 2019, doi: 10.1007/s11277-019-06921-x.

[12] L. Amhaimar, S. Ahyoud, A. Elyaakoubi, A. Kaabal, K. Attari, and A. Asselman, “PAPR Reduction Using Fireworks Search Optimization Algorithm in MIMO-OFDM Systems,” Journal of Electrical and Computer Engineering, vol. 2018, pp. 1–11, Sep. 2018, doi:10.1155/2018/3075890.

[13] T. Udomsripaiboon, “Adjustable dynamic range for PAPR clipping technique in large-scale MIMO-OFDM systems,” 2018 International ECTI Northern Section Conference on Electrical, Electronics, Computer and Telecommunications Engineering (ECTI-NCON), Feb. 2018, doi: 10.1109/ecti-ncon.2018.8378275.

[14] B. D. Timande and Dr. M. K. Nigam, “PAPR Reduction an effective approach for next frontier MIMO-OFDM systems,” Journal of Engineering Research, vol. 9, Oct. 2021, doi: 10.36909/jer.11379.

[15] Y. Moegiharto, A. M. Kautsar Bebyrahma, and I. Anisah, “BER Performance of Joint PTS PAPR Reduction Technique and Wiener HPA Predistortion in OFDM System,” 2019 International Electronics Symposium (IES), Sep. 2019, doi: 10.1109/elecsym.2019.8901566.

[16] M. D. N. Habibah, G. S. Palupi, A. A. Puspitasari, U. A. Nadhiroh, M. Ridwan, and Y. Moegiharto, “Performance of a Joint PAPR Reduction Clipping and Filtering (CF) Scheme and Predistortion Techniques in Amplify and Forward (AF) Relaying System with Relay Selection Strategy,” 2021 International Electronics Symposium (IES), Sep. 2021, doi: 10.1109/ies53407.2021.9594005.

[17] A. Syarif, Arifin, N. Sa’adah, I. G. P. Astawa, and Y. Moegiharto, “Performance of Joint PAPR Reduction Iterative Clipping and Filtering (ICF) and Predistortion in OFDM Systems Using Software Defined Radio,” 2021 International Electronics Symposium (IES), Sep. 2021, doi: 10.1109/ies53407.2021.9593971.

[18] M. W. Gunawan, N. A. Priambodo, M. M. Gulo, A. Arifin, Y. Moegiharto, and H. Briantoro, “Evaluations of the predistortion technique by neural network algorithm in MIMO-OFDM system using USRP,” JURNAL INFOTEL, vol. 14, no. 4, pp. 287–293, Nov. 2022, doi: 10.20895/infotel.v14i4.825.

[19] M. M. Gulo, I. G. P. Astawa, and A. Sudarsono, “Performance Analysis of MIMO-OFDM System Using Predistortion Neural Network with Convolutional Coding Addition to Reduce SDR-Based HPA Nonlinearity,” EMITTER International Journal of Engineering Technology, pp. 35–59, Jun. 2023, doi: 10.24003/emitter.v11i1.791.

[20] M. M. Gulo, I. G. P. Astawa, A. Sudarsono, N. A. Priambodo, and M. W. Gunawan, “Implementation of Tiny Machine Learning (TinyML) as Pre-distorter for High Power Amplifier (HPA)Linearization of SDR-based MIMO-OFDM,” 2023 International Electronics Symposium (IES), Aug. 2023, doi: 10.1109/ies59143.2023.10242459.

[21] M. H. Lee, M. B. Shahab, M. F. Kader, and S. Y. Shin, “Spatial multiplexing using walsh-hadamard transform,” 2016 International Conference on Smart Green Technology in Electrical and Information Systems (ICSGTEIS), Oct. 2016, doi: 10.1109/icsgteis.2016.7885764.

[22] L. Kansal, V. Sharma, and J. Singh, “Multiuser Massive MIMO-OFDM System Incorporated with Diverse Transformation for 5G Applications,” Wireless Personal Communications, vol. 109, no. 4, pp. 2741–2756, Aug. 2019, doi: 10.1007/s11277-019-06707-1.

[23] Y. Tian and M. E. Magaña, “Pilot-Aided Channel Estimation for Massive MIMO Systems in TDD-mode Using Walsh-Hadamard Transformed Subsampled Data at the Base Station,” Wireless Personal Communications, vol. 119, no. 1, pp. 423–440, Mar. 2021, doi:10.1007/s11277-021-08218-4.

[24] S. Bharati and P. Podder, “Adaptive PAPR Reduction Scheme for OFDM Using SLM with the Fusion of Proposed Clipping and Filtering Technique in Order to Diminish PAPR and Signal Distortion,” Wireless Personal Communications, vol. 113, no. 4, pp. 2271–2288, Apr. 2020, doi: 10.1007/s11277-020-07323-0.

[25] K. Anoh, C. Tanriover, and B. Adebisi, “On the Optimization of Iterative Clipping and Filtering for PAPR Reduction in OFDM Systems,” IEEE Access, vol. 5, pp. 12004–12013, 2017, doi:10.1109/access.2017.2711533.

[26] H. Al-Kanan and F. Li, “A Simplified Accuracy Enhancement to the Saleh AM/AM Modeling and Linearization of Solid-State RF Power Amplifiers,” Electronics, vol. 9, no. 11, p. 1806, Oct. 2020, doi:10.3390/electronics9111806.

[27] A. E. Jayati, Wirawan, T. Suryani, and Endroyono, “Characteristic of HPA Nonlinear Distortion Effects in MIMO-GFDM Systems,” 2018 International Conference on Information and Communication Technology Convergence (ICTC), Oct. 2018, doi:10.1109/ictc.2018.8539527.

[28] C. An and H.-G. Ryu, “Design and Performance Comparison of W-OFDM Under the Nonlinear HPA Environment,” Wireless Personal Communications, vol. 98, no. 1, pp. 983–999, Aug. 2017, doi:10.1007/s11277-017-4904-x.

[29] A. E. Jayati and M. Sipan, “Impact of Nonlinear Distortion with the Rapp Model on the GFDM System,” 2020 Third International Conference on Vocational Education and Electrical Engineering (ICVEE), Oct. 2020, doi: 10.1109/icvee50212.2020.9243295.

[30] L. Xu, F. Gao, W. Zhang, and S. Ma, “Model Aided Deep Learning Based MIMO OFDM Receiver With Nonlinear Power Amplifiers,” 2021 IEEE Wireless Communications and Networking Conference (WCNC), Mar. 2021, doi: 10.1109/wcnc49053.2021.9417512.

[31] Z. Li, S. Perera, Y. Zhang, G. Zhang, and R. Doviak, “Phased-Array Radar System Simulator (PASIM): Development and Simulation Result Assessment,” Remote Sensing, vol. 11, no. 4, p. 422, Feb. 2019, doi: 10.3390/rs11040422.

[32] A. Jayati et al., “Partial Transmit Sequence and Selected Mapping Schemes for PAPR Reduction in GFDM Systems,” International Journal of Intelligent Engineering and Systems, vol. 12, no. 6, pp. 114–122, Dec. 2019, doi: 10.22266/ijies2019.1231.11.

[33] “Maximum Likelihood SNR Estimation for QAM Signals Over Slow Flat Fading Rayleigh Channel,” KSII Transactions on Internet and Information Systems, Nov. 2016, doi: 10.3837/tiis.2016.11.009.